

1       **Title: Marine biomarkers from ice cores reveal enhanced high-latitude**

2               **Southern Ocean carbon sink during the Antarctic Cold Reversal**

3

4

5

6

7

8       This is a non-peer reviewed EarthArXiv pre-print in review in

9                               *Nature Geoscience*

10

11

12

13

14

15

16

17

18

19

20

21

22

23           **Title: Marine biomarkers from ice cores reveal enhanced high-latitude**  
24                   **Southern Ocean carbon sink during the Antarctic Cold Reversal**

25  
26 **Authors:** C.J. Fogwill\*<sup>1,2</sup>, C.S.M. Turney<sup>2,3,4</sup>, L. Menviel<sup>4</sup>, A. Baker<sup>2</sup>, M. E. Weber<sup>5</sup>, B. Ellis<sup>6</sup>,  
27 Z.A. Thomas<sup>2,3,4</sup>, N. R. Golledge<sup>7,8</sup>, D. Etheridge<sup>9</sup>, M. Rubino<sup>1,9,10</sup>, D.P. Thornton<sup>9</sup>, T.D. van  
28 Ommen<sup>11,12</sup>, A.D. Moy<sup>11,12</sup>, M.A.J. Curran<sup>11,12</sup>, S. Davies<sup>13</sup>, M.I. Bird<sup>3,14</sup>, N.C. Munksgaard<sup>14,15</sup>,  
29 C.M. Rootes<sup>16</sup>, H. Millman<sup>1,4</sup>, J. Vohra<sup>2</sup>, A. Rivera<sup>17</sup>, A. Mackintosh<sup>18</sup>, J. Pike<sup>19</sup>, I.R. Hall<sup>19</sup>, E.A.  
30 Bagshaw<sup>19</sup>, E. Rainsley<sup>1</sup>, C. Bronk Ramsey<sup>20</sup>, M. Montinari<sup>1</sup>, A. Cage<sup>1</sup>, M. Harris<sup>1</sup>, R. Jones<sup>21†</sup>,  
31 A. Power<sup>21</sup>, J. Love<sup>21</sup>, J. Young<sup>22</sup>, L.S. Weyrich<sup>3,22</sup>, A. Cooper<sup>3,22</sup>

32 **Affiliations:**

33 <sup>1</sup>School of Geography, Geology and the Environment, University of Keele, Staffordshire, UK

34 <sup>2</sup>Palaeontology, Geobiology and Earth Archives Research Centre, School of Biological Earth and  
35 Environmental Sciences, University of New South Wales, 2052, Australia

36 <sup>3</sup>ARC Centre of Excellence in Australian Biodiversity and Heritage

37 <sup>4</sup>Climate Change Research Centre, School of Biological Earth and Environmental Sciences,  
38 University of New South Wales, 2052, Australia

39 <sup>5</sup>Steinmann Institute, University of Bonn, Poppelsdorfer Schloss, Bonn, Germany

40 <sup>6</sup>Research School of Earth Sciences, Australian National University, Canberra, Australia

41 <sup>7</sup>Antarctic Research Centre, Victoria University of Wellington, Wellington 6140, New Zealand

42 <sup>8</sup>GNS Science, Lower Hutt, 5001, New Zealand

43 <sup>9</sup>CSIRO Oceans and Atmosphere, Aspendale, Victoria, 3195 Australia

44 <sup>10</sup>Dipartimento di Matematica e Fisica, Università della Campania "Luigi Vanvitelli", viale  
45 Lincoln, 5-81100 Caserta, Italy

46 <sup>11</sup>Department of the Environment, Australian Antarctic Division, 203 Channel Highway,  
47 Kingston, Tasmania 7050, Australia

48 <sup>12</sup>Antarctic Climate & Ecosystems Cooperative Research Centre, University of Tasmania,  
49 Private Bag 80, Hobart, Tasmania 7001, Australia

50 <sup>13</sup>Department of Geography, Swansea University, Swansea, United Kingdom

51 <sup>14</sup>Centre for Tropical Environmental and Sustainability Science, College of Science, Technology  
52 and Engineering, James Cook University, Cairns, Australia

53 <sup>15</sup>Research Institute for the Environment and Livelihoods, Charles Darwin University, Australia

54 <sup>16</sup>Department of Geography, University of Sheffield, United Kingdom

55 <sup>17</sup>Glaciology and Climate Change Laboratory, Centro de Estudios Científicos, Valdivia, Arturo Prat  
56 514, Chile

57 <sup>18</sup>School of Earth, Atmosphere and Environment, Monash University, Melbourne, Australia

58 <sup>19</sup>School of Earth and Ocean Sciences, University of Cardiff, Wales, UK

59 <sup>20</sup>Research Laboratory for Archaeology and the History of Art, University of Oxford, Dyson  
60 Perrins Building, South Parks Road, Oxford, OX1 3QY, UK

61 <sup>21</sup> BioEconomy Centre, The Henry Wellcome building for Biocatalysis, Biosciences, Stocker  
62 Road, Exeter University, Exeter, EX4 4QD, UK

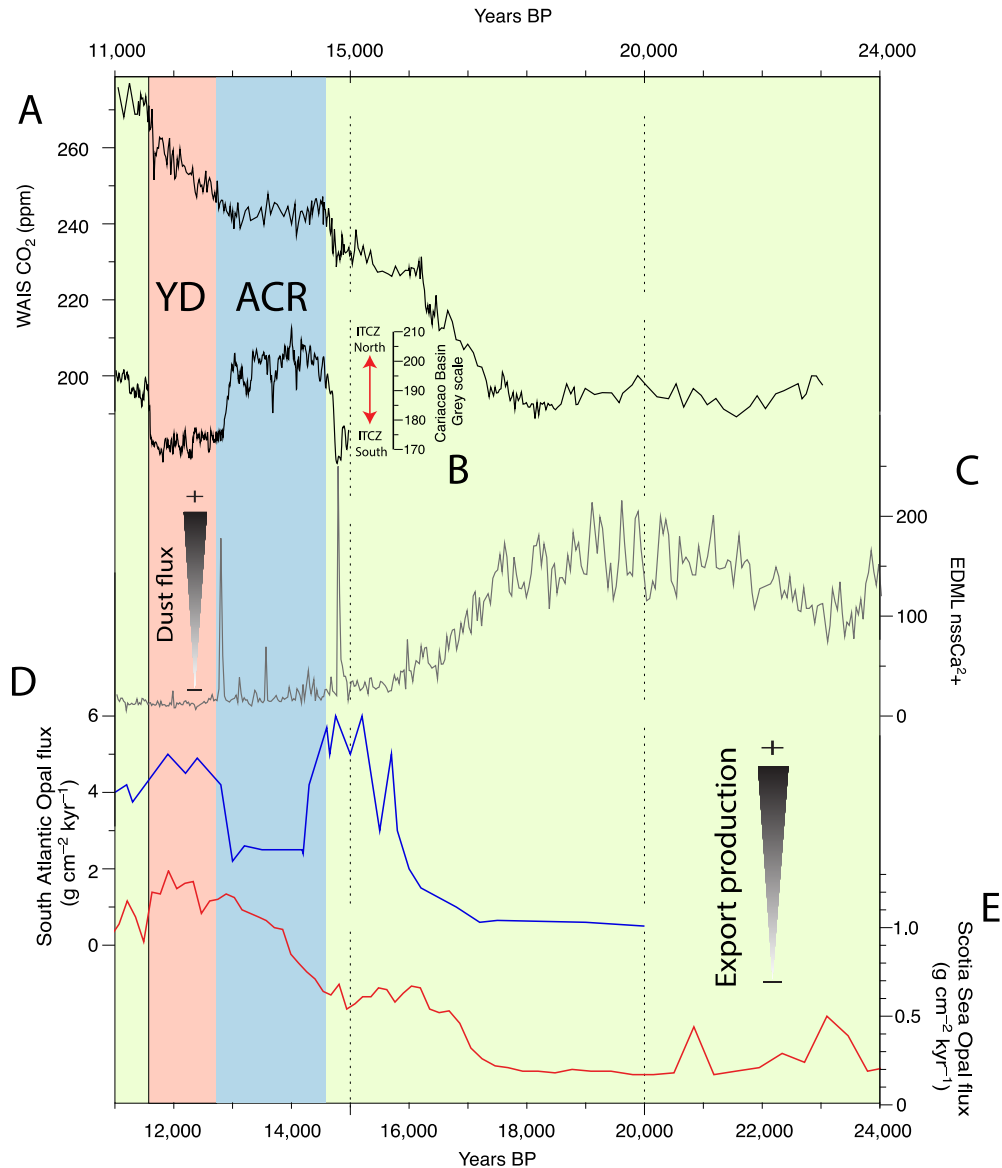
63 <sup>22</sup>Australian Centre for Ancient DNA, University of Adelaide, 5005, Australia

64 Contact Information: \*Correspondence to [c.j.fogwill@keele.ac.uk](mailto:c.j.fogwill@keele.ac.uk)

65 **Abstract: The Southern Ocean plays a fundamental role in regulating global atmospheric**  
66 **CO<sub>2</sub> levels, yet the underlying processes and feedbacks that control the carbon cycle today**  
67 **remain unclear. The Last Glacial Transition (LGT 18,000-11,000 years ago or 18-11 kyr BP)**  
68 **experienced rapid and sustained changes in CO<sub>2</sub> that may provide fresh insights, however,**  
69 **fundamental questions over the mechanism(s) that modulate climate-carbon dynamics**  
70 **during this important period remain. One key example is the enigmatic 1,900-year plateau**  
71 **that interrupted the rise in atmospheric CO<sub>2</sub> during the LGT during a period of pronounced**  
72 **mid- to high-latitude Southern Hemisphere cooling termed the Antarctic Cold Reversal**  
73 **(ACR, 14,600-12,700 years ago or 14.6-12.7 kyr BP). Here we utilise five independent**  
74 **approaches to provide a detailed marine biomarker reconstruction from a highly-resolved**  
75 **Antarctic ‘horizontal’ ice core. Our reconstruction provides a coherent signal of enhanced**  
76 **surface ocean productivity and microbial diversity, in the form of marine picoeukaryotes**  
77 **and nanoplankton, that have been captured within ice from precipitation derived from the**  
78 **South Atlantic sector of the high-latitude Southern Ocean. When combined with marine**  
79 **sediment records, we confirm this period was coincident with increased biological export**  
80 **(driving CO<sub>2</sub> sequestration), suggesting high-latitude biological feedbacks contributed to the**  
81 **ACR CO<sub>2</sub> plateau. Transient climate modelling indicates that this period coincided with the**  
82 **maximum seasonal variability in sea-ice extent, implying sea-ice feedbacks enhanced CO<sub>2</sub>**  
83 **sequestration, making the high-latitude South Atlantic sector Southern Ocean a significant**  
84 **carbon sink that contributed to the sustained plateau in CO<sub>2</sub> levels during the ACR. This**  
85 **finding has ramifications for our understanding of contemporary ice-ocean-carbon**  
86 **feedbacks, and confirms the dynamic role Antarctic sea ice plays, providing a negative**  
87 **feedback during periods of rising CO<sub>2</sub>, a result that requires detailed assessment given recent**

88 **high-latitude sea ice changes, that may impact the efficiency of the Southern Ocean carbon**  
89 **sink.**

90 **Introduction:** The Southern Ocean occupies some 14% of the planet's surface and plays a  
91 fundamental role in the global carbon cycle and climate (Bauska et al., 2016; Le Quéré et al., 2007;  
92 Marshall and Speer, 2012). It provides a direct connection to the deep ocean carbon reservoir  
93 through physical and biological processes that include surface primary productivity,  
94 remineralisation of carbon at depth, and upwelling of carbon-rich and radiocarbon ( $^{14}\text{C}$ )-depleted  
95 water masses (Gottschalk et al., 2016; Marshall and Speer, 2012; Turney et al., 2016). However,  
96 the role of these different processes in modulating past and future air-sea carbon flux remains  
97 poorly understood (Hewitt et al., 2016; Schmitt et al., 2012). Considerable uncertainty surrounds  
98 the source(s) and sink(s) of carbon during the Last Glacial Termination (LGT; 19 to 11.6 kyr BP)  
99 when atmospheric  $\text{CO}_2$  rose from approximately 190 parts per million (ppm) to around 270 ppm  
100 (Figure 1). Recent detailed analysis of the stable isotopic composition of atmospheric carbon  
101 dioxide ( $\delta^{13}\text{C}-\text{CO}_2$ ) from Antarctic ice cores provides new insights into the potential effects of  
102 terrestrial carbon in defining rapid rises in  $\text{CO}_2$ , but highlighted that  $\text{CO}_2$  variability across this  
103 period may reflect a combination of sources, sinks and feedbacks (Bauska et al., 2016), that may  
104 provide valuable insights into the role of the Southern Ocean processes in modulating global  $\text{CO}_2$   
105 today (Barnes, 2015).



106

107 **Figure 1.** Comparison of A. Atmospheric CO<sub>2</sub> concentration from the WAIS divide core (WD<sub>2014</sub>  
 108 chronology) (Marcott et al., 2014) with available Southern Hemisphere records of B. Cariaco  
 109 Basin grey scale, a measure of latitudinal changes in the trade winds associated with the ITCZ  
 110 (Hogg et al., 2016). C. non-sea salt Ca<sup>2+</sup> flux (nssCa<sup>2+</sup>) from EPICA Dronning Maud Land  
 111 (EDML) (Wolff et al., 2006a). D. South Atlantic opal flux from core TN057-13 (Anderson et al.,  
 112 2009). E. Scotia Sea opal flux from core MD07-3134 (Weber et al., 2014). Vertical boxes indicate  
 113 the periods defined by the Antarctic Cold Reversal (ACR) (blue), the Younger Dryas (YD)

114 chronozone (11.7-12.7 kyr BP).

115

116 The parallel changes in Antarctic temperature and atmospheric CO<sub>2</sub> have been interpreted as  
117 climate playing a substantial role in the carbon budget of the Southern Ocean (Anderson et al.,  
118 2009; Monnin et al., 2001). Several physical and biological mechanisms have been invoked to  
119 explain these observations. These include changes in the strength and/or latitudinal migration of  
120 the mid-latitude Southern Hemisphere jet stream and prevailing surface westerly air flow that  
121 drives Southern Ocean overturning (Anderson et al., 2009; Marshall and Speer, 2012; Toggweiler  
122 et al., 2006), variations in iron (dust) fertilization of subantarctic phytoplankton impacting the  
123 efficiency of the Southern Ocean biological carbon pump (Jaccard et al., 2016; Jaccard et al., 2013;  
124 Martínez-García et al., 2014), Antarctic sea-ice controlling CO<sub>2</sub> exchange (Butterworth and Miller,  
125 2016; Delille et al., 2014) and carbon drawdown (Barnes, 2015), as well as the potential impacts  
126 of a warming ocean on CO<sub>2</sub> exchange (Bauska et al., 2016). The role of the Southern Ocean as a  
127 source or sink of atmospheric carbon during the LGT remains highly contested, with the above  
128 processes not fully accounting for the pattern of change in CO<sub>2</sub> recorded over this period (Jaccard  
129 et al., 2016), implying that one or more mechanisms are currently not captured in our present  
130 understanding.

131

132 One striking feature of the LGT record is a 1,900 year-long-plateau in CO<sub>2</sub> concentration, when  
133 CO<sub>2</sub> paused at a near-constant 240 ppm coinciding with the period of high latitude Southern  
134 Hemisphere surface cooling, termed the Antarctic Cold Reversal (ACR; 14.6-12.7 kyr BP) (Pedro  
135 et al., 2015). Whilst the rapid rises in CO<sub>2</sub> may be attributed to either terrestrial carbon feedbacks  
136 or through shifts in the Intertropical Convergence Zone (ITCZ) that may have impacted ocean

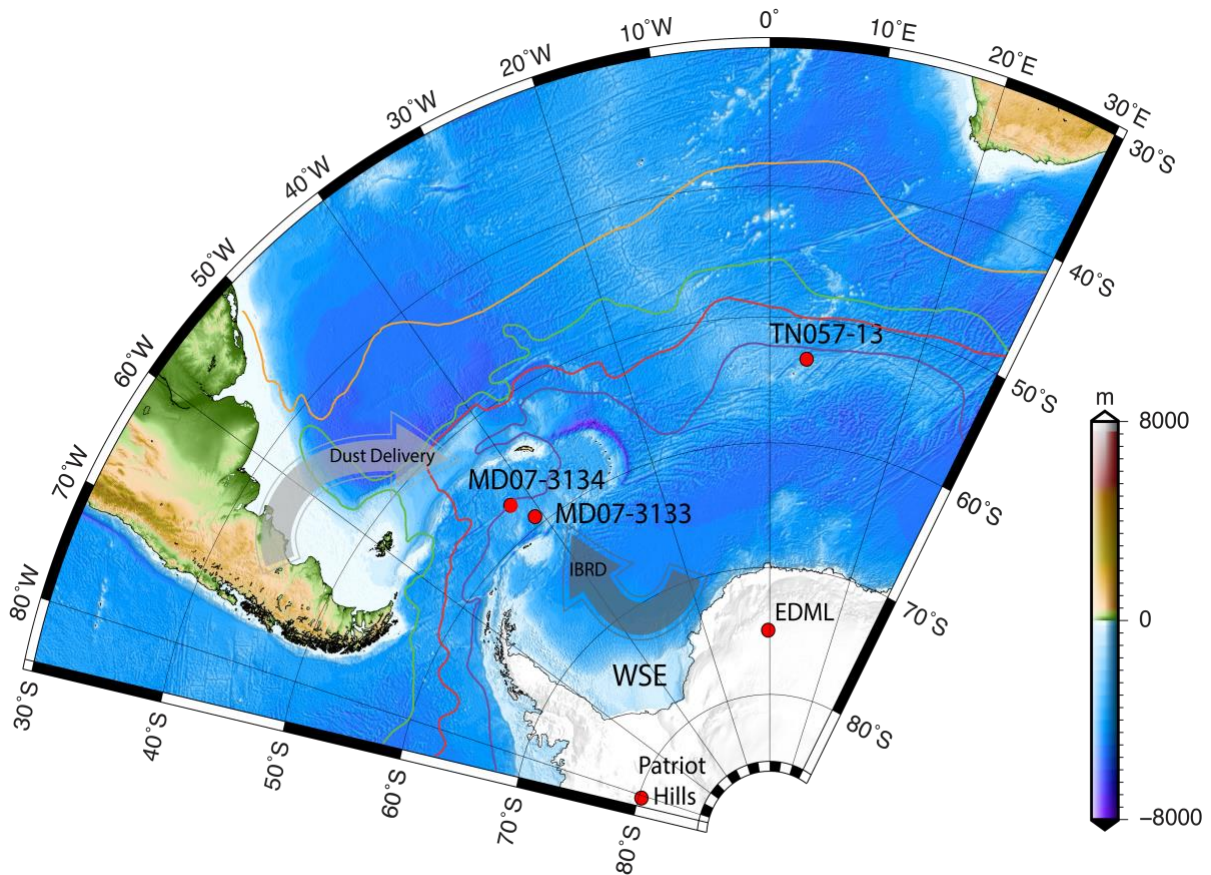
137 circulation and the location and intensity of the Southern Hemisphere Westerlies (Bauska et al.,  
138 2016), the enigmatic plateau between 14.6-12.7 kyr BP remains unexplained (Figure 1). In the  
139 absence of clear mechanisms the need for well resolved palaeo-proxy reconstructions that may  
140 shed light on causes of this plateau are needed, as it may help reveal new insights into the high-  
141 latitude ocean's potential for carbon sequestration (Boyd et al., 2019). Here we exploit an  
142 innovative new ice core record to reconstruct high-latitude environmental changes during the ACR  
143 to gain new insights into the driver (s) of Southern Ocean carbon feedbacks during this important  
144 transition.

145

146 The ACR was characterized by surface cooling across the mid to high-latitude Southern  
147 Hemisphere (Fogwill and Kubik, 2005; McGlone et al., 2010; Pedro et al., 2015), coincident with  
148 sustained warming across the Northern Hemisphere (the North Atlantic Bølling-Allerød  
149 interstadial) (Jaccard et al., 2016; Marcott et al., 2014), abrupt global sea level rise (Fogwill et al.,  
150 2017; Weber et al., 2014), and major disruptions to atmospheric and ocean circulation, and the  
151 carbon cycle (Jaccard et al., 2016; Martínez-García et al., 2014; Schmitt et al., 2012). Whilst the  
152 global sequence of events during the ACR is reasonably well known (Pedro et al., 2015), a clear  
153 understanding of the drivers and impacts of contrasting polar climate changes on global CO<sub>2</sub> trends  
154 has proved elusive due to the challenges in precisely aligning ice and marine records across this  
155 period (Jaccard et al., 2016). In part this reflects the lack of well-resolved, high accumulation  
156 marine sedimentary records from the high-latitude Southern Ocean. One crucial record in this  
157 regard comes from marine sediment core TN057-13 (~53°S) (Anderson et al., 2009; Jaccard et al.,  
158 2016) (Figure 2), which suggests that the ACR was characterized by reduced carbon sequestration  
159 in the mid-latitudes (as measured by decreased biological productivity or export production



160 (Anderson et al., 2009; Gottschalk et al., 2016); Figure 1D), possibly the result of enhanced  
161 stratification that decreased the vertical supply of nutrients across the high-nutrient, low-  
162 chlorophyll (HNLC) sectors of the Southern Ocean during cooling (Anderson et al., 2009).  
163 However, such a hypothesis is difficult to test in the absence of other well resolved, high-latitude  
164 records of Southern Ocean productivity.



165  
166 **Figure 2.** Location map of the South Atlantic sector of the Southern Ocean with the locations of  
167 Patriot Hills in the Ellsworth Mountains, the EPICA Dronning Maud Land (EDML) ice core  
168 (Wolff et al., 2006a), the Scotia Sea MD07-3134 core (Weber et al., 2014), and marine core  
169 TN057-13 (Anderson et al., 2009) produced with GMT (Wessel, 1998). Locations of the southern  
170 limb of the Antarctic Circumpolar Current (purple), the polar front (red), subantarctic front (green)  
171 and the subtropical front (yellow) (Orsi et al., 1995).

172 Changes in Southern Ocean productivity polewards of TN057-13 are recorded within the highly-  
173 resolved marine core MD07-3134, located at  $\sim 59^{\circ}\text{S}$  in the Scotia Sea (Figure 1E; see  
174 Supplementary Information) (Weber et al., 2014). In common with core TN057-13 this sequence  
175 is exceptionally well resolved, with sedimentation rates of 20 to 200 cm/kyr (Weber et al., 2014).  
176 Here we report opal burial rates from MD07-3134 used, after accounting for sediment focussing  
177 with  $^{230}\text{Th}$  normalisation (see Supplementary Information) (Meyer-Jacob et al., 2014), we estimate  
178 changes in biological productivity (export production) at the site (Figure 1E). The reconstruction  
179 suggests that whilst export production in the high-latitude Southern Ocean similarly increased  
180 from  $\sim 17$  ka, the trend was maintained through the ACR, in antiphase to records further north  
181 (Anderson et al., 2009) (Figure 1 and Figure 2), suggesting that at high latitudes other driver(s) of  
182 marine biological activity may have operated during this period. In the absence of a network of  
183 highly resolved marine records from the high-latitude Southern Ocean that have been normalised  
184 for sedimentation rate changes (through  $^{230}\text{Th}$  normalisation (see Supplementary Information))  
185 (Sprenk et al., 2013), we develop a new record of high-latitude surface ocean productivity using  
186 the marine biomarkers and DNA analyses of picoplankton and nanoplankton from a highly-  
187 resolved horizontal ice core from the Weddell Sea Embayment, Antarctica (Fogwill et al., 2017),  
188 that captures regional-scale processes operating across the south Atlantic sector of the Southern  
189 Ocean across the LGT (Figure 3) (Fogwill et al., 2017; Turney et al., 2013).

## 190 **Materials and methods**

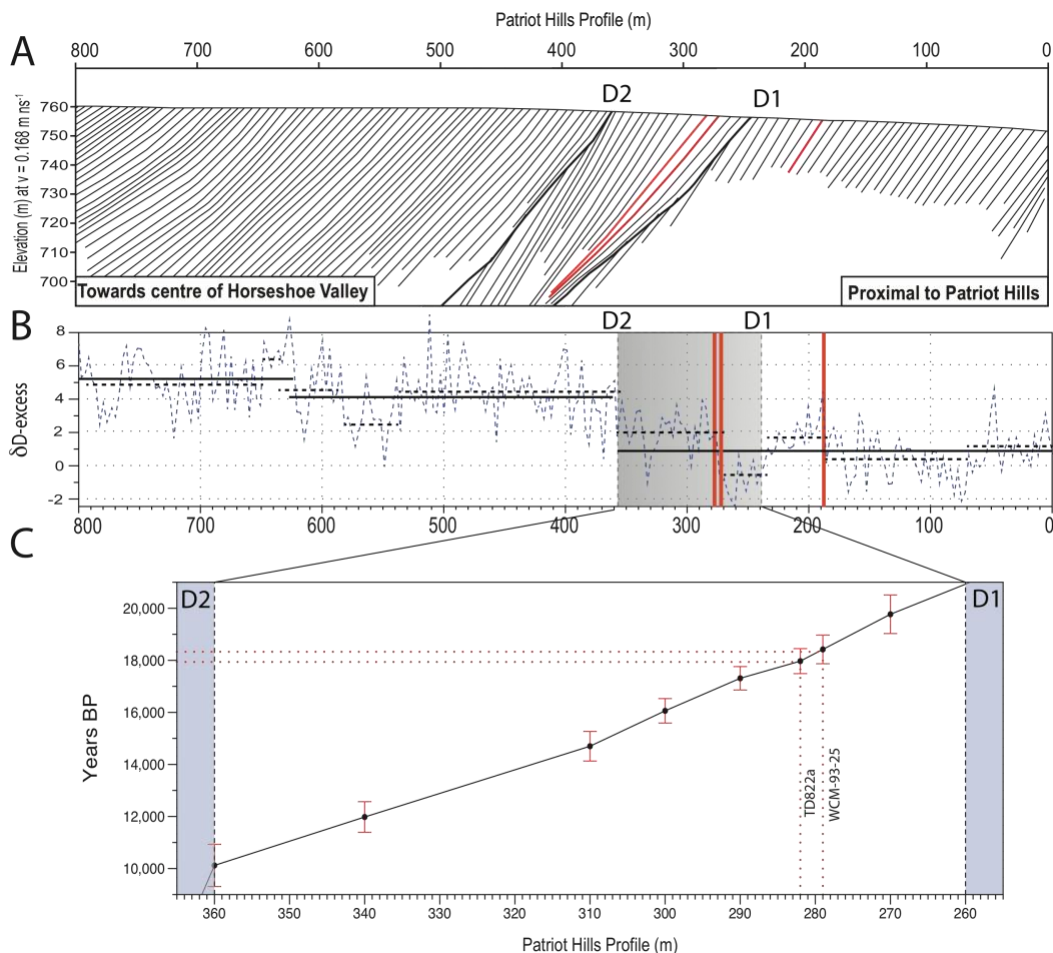
191 The ‘horizontal’ ice core record was obtained from the exposed blue ice area (BIA) at Patriot Hills  
192 in Horseshoe Valley, Ellsworth Mountains (Figure 2) (Fogwill et al., 2017), which, in contrast to  
193 many other BIA areas has not been mixed through ice flow (Fogwill et al., 2017; Winter et al.,  
194 2016a). Horseshoe Valley is a locally-sourced compound glacier that is buttressed by, but

195 ultimately coalesces with, the Institute Ice Stream close to the contemporary grounding line of the  
196 AIS making it the ideal site to build up a record of environmental and ice sheet change in this  
197 sector of Antarctica (Fogwill et al., 2017). With contemporary snow accumulation at the site being  
198 associated with low-pressure systems that have either tracked across the Weddell Sea from the  
199 southern Atlantic Ocean, or that relate to blocking by the Antarctic Peninsula (Abram et al., 2007;  
200 Reijmer et al., 1999; Turney et al., 2013), the site is ideally placed to record environmental changes  
201 across the Scotia Sea, Weddell Sea and high-latitude South Atlantic (Figure 2).

202

203 The Patriot Hills record is chronologically constrained by multiple greenhouse gas species (CO<sub>2</sub>,  
204 CH<sub>4</sub> and N<sub>2</sub>O) supported by geochemically identified volcanic (tephra) horizons (Figure 3 and  
205 Supplementary Information), with increased sampling and more tephra's identified providing  
206 tighter chronological control through the LGT building on previous studies (Fogwill et al., 2017).  
207 The age model demonstrates that the BIA sequence spans from ~2.5 to 50 kyr BP, with two  
208 unconformities (Discontinuities D1 and D2), that mark the build-up to (D1), and deglaciation from  
209 (D2), the last glacial cycle (Figure 3) (Fogwill et al., 2017). High-resolution ground penetrating  
210 radar (Winter et al., 2016b) and detailed analysis of trace gases and volcanic tephra horizons  
211 (Fogwill et al., 2017) demonstrates that the conformable BIA layers or 'isochrons' between these  
212 two unconformities span the period between ~11 to ~23 kyr BP (Figure 3C). Thus the horizontal  
213 ice core captures a unique highly-resolved record of ice-sheet dynamics (Fogwill et al., 2017), in  
214 an area of exceptionally slow moving ice, with no chronological breaks or unconformities across  
215 the LGT (see Supplementary Information), providing an opportunity to obtain large volume ice  
216 samples of known ages for innovative multiproxy biomarker analyses (Fogwill et al., 2017).

217

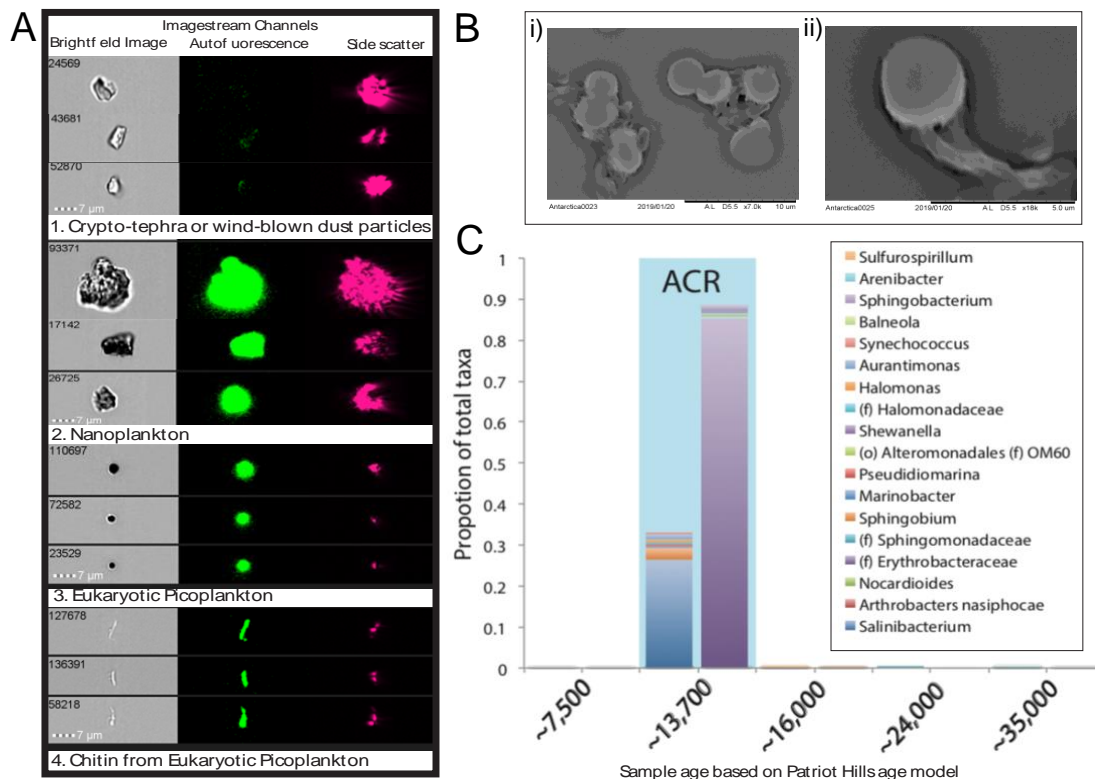


218  
 219 **Figure 3.** A. Schematic stratigraphic succession from Ground Penetrating Radar (GPR), across the  
 220 Patriot Hills BIA, indicating ice accumulation punctuated by two periods of erosion (D1 and D2;  
 221 thick black lines), and the position of tephras at 282m, 279m and 190m (red lines) across the profile  
 222 (Fogwill et al., 2017). B. Dashed blue line represents  $\delta D$ -excess across profile; solid horizontal  
 223 black lines denote potential regime shifts across the profile at 99% confidence, and dashed black  
 224 lines denote potential regime shifts across the profile at 95% confidence (Rodionov, 2004). C.  
 225 Age-depth model based upon chronological control ties between D1 ~21 ka (21,000 years) and D2  
 226 ~10 ka (10,000 years) as defined from volcanic ‘tephra’ horizons and most-likely age as derived  
 227 from multiple trace gas comparison ( $\text{CH}_4$ ,  $\text{CO}_2$ ,  $\text{N}_2\text{O}$ ; see Supplementary Information (Fogwill et

228 al., 2017)).

229

230 To examine regional environmental responses through the LGT, fluorescent organic matter (fOM)  
231 content and liquid chromatography organic carbon detection (LC-OCD) (Huber et al., 2011)  
232 analysis of biomarkers was undertaken on LGT ice outcropping at the Patriot Hills BIA (see  
233 Supplementary Information and Figure 4) (Huber et al., 2011). Detailed analysis of the  
234 fluorescence emission spectra identified two protein-like components (Stedmon et al., 2003) in ice  
235 throughout the profile. Due to their excitation-emission wavelengths, we can unambiguously  
236 identify these fOM components as those widely reported in precipitation as TRY LIS and TY LIS:  
237 tryptophan and tyrosine-like substances (Jørgensen et al., 2011; Parlanti et al., 2000) (see  
238 Supplementary Information (Figure S2)). Whilst there are limited studies in ancient Antarctic ice  
239 (D'Andrilli et al., 2016), past studies have demonstrated that a strong TRY LIS signal is found in  
240 Antarctic snow and ice derived from precipitation from the marine environment (Barker et al.,  
241 2013; Hood et al., 2009; King et al., 2019; Rohde et al., 2008; Smith et al., 2017).



242  
 243 **Figure 4.** A. Imaging Flow Cytometry (ImageSteam®) analysis highlights the four principal  
 244 populations identified in ancient ice from the Patriot Hills BIA. B. SEM images of marine  
 245 picoeukaryotes with tails (chitin) C. Microorganisms previously identified in marine seawater  
 246 (teal) or marine sediments (light blue) are observed in samples from different sections of the Patriot  
 247 Hills BIA. The proportion of the taxa from each core, given a specific extraction method  
 248 (Powerlyzer left hand side, or CTAB, right hand side). The period defined by the ACR is  
 249 represented by the blue box.

250  
 251 To unambiguously identify the source of the fOM signal and confirm our interpretation of a marine  
 252 origin we apply Imaging Flow Cytometry (ImageSteam®) and Scanning Electron Microscopy  
 253 (SEM) to ancient ice samples. Imaging Flow Cytometry reveals four significant populations  
 254 preserved within ice from samples in the Patriot Hills BIA record (Figure 4A). The first is an

255 inorganic fraction ranging from ~2-10 $\mu$ m in length, characterised by a flaky flat structure and no  
256 autofluorescence, which we interpret as a mixture of crypto-tephra, and / or wind-blown dust. The  
257 second population is composed of dark angular particles ~5-12 $\mu$ m in length, that have a high  
258 autofluorescence, and a 3-D structure evidenced from a strong ch006 (side scatter) signal, which  
259 we classify as nanoplankton. The third population is characterised by spheroidal forms ranging in  
260 diameter from ~2-5 $\mu$ m, that again have a high autofluorescence, and a 3-D structure evidenced  
261 from a strong ch006 (side scatter) signal, which we identify as Eukaryotic picoplankton and  
262 picoeukaryotes. Finally, a fourth population is characterised by elongate spicules or rods between  
263 2-10 $\mu$ m, that have a high autofluorescence, and a 3-D structure evidenced from a strong ch006  
264 (side scatter) signal, which we identify as Chitin, most likely related to the third population of  
265 eukaryotic picoplankton and picoeukaryotes, an interpretation confirmed through SEM (Figure  
266 4B). Beyond these four populations only a few other events were recorded, which were identified  
267 as broken diatom frustules, which were characterised by a high autofluorescence, and a side scatter  
268 signal (see Supplementary Information).

269  
270 Of the populations identified through Imaging Flow Cytometry (ImageStream®) the eukaryotic  
271 picoplankton and picoeukaryotes and Chitin populations made up most the made ~56% of the total,  
272 with the non-fluorescent signal ~12%, and finally ~36% of the signal being less than <2 $\mu$ m,  
273 therefore unclassified at present (Classification of this fine particulate fraction is difficult due to  
274 its small size. However, ~20 % of events within this fraction are characteristic of picoeukaryotes  
275 (displaying similar properties to eukaryotic picoplankton identified in the > 2  $\mu$ m fraction, below).  
276 The remaining 80 % is comprised of 'elongate fluorescent rods' (likely chitin), and unclassified  
277 angular and round particulate.

278

279 The fact that the picoplankton and picoeukaryotes populations ( $>2\mu\text{m}$ ) were not recorded as one  
280 population in the Imaging Flow Cytometry (ImageStream®) analysis was concerning, and likely  
281 reflects the process of the flow cytometry, where sheath fluids run through the machine at the same  
282 time as the sample – this focuses the sample in a steady stream, so that each ‘event’ can be analysed  
283 individually. This effect, or possibly vortexing prior to analysis, may have disaggregated the  
284 picoplankton and picoeukaryotes, separating the tails (chitin) from the spheroidal ‘body’ (see  
285 Supplementary Information). To test this Scanning Electron Microscopy (SEM) was undertaken  
286 on samples that had not been previously unfrozen or analysed. SEM imaging demonstrated  
287 unambiguously that whole picoplankton and picoeukaryotes were present in the water samples  
288 from ancient ice, complete with chitin (Figure 4B).

289

290 Having undertaken four independent yet mutually supportive biomarker approaches on ice samples  
291 across the LGT from the Patriot Hills BIA we can conclude that marine biomarkers are present  
292 throughout the profile. The location of the BIA, the unambiguous nature of the biomarker signal,  
293 and the observation that marine regions have exceptionally low humic-like substances (HULIS)  
294 content and relatively high TRY LIS content (Muller et al., 2008; Willey, 2000), indicates that the  
295 primary source of fOM in the ice is from precipitation derived from the high-latitude Southern  
296 Ocean (Abram et al., 2007; Reijmer et al., 1999; Turney et al., 2013). This interpretation is  
297 supported by both independent LC-OCD and independent fluorescence techniques (see Figure 4  
298 and Supplementary Information (Figure S2)), which fail to identify the presence of humic-like  
299 substances in ice from the Patriot Hills BIA, ruling out either a terrestrial source of the fOM signal  
300 or *in situ* secondary production (Smith et al., 2017) in the ancient ice which was recovered from



301 depth. Imaging Flow Cytometry (ImageStream®) identifies that the bulk of the fOM signal relates  
302 to the presence of microscopic marine plankton, principally picoplankton and picoeukaryotes, but  
303 also with nanoplankton populations up to ~8µm in size.

304

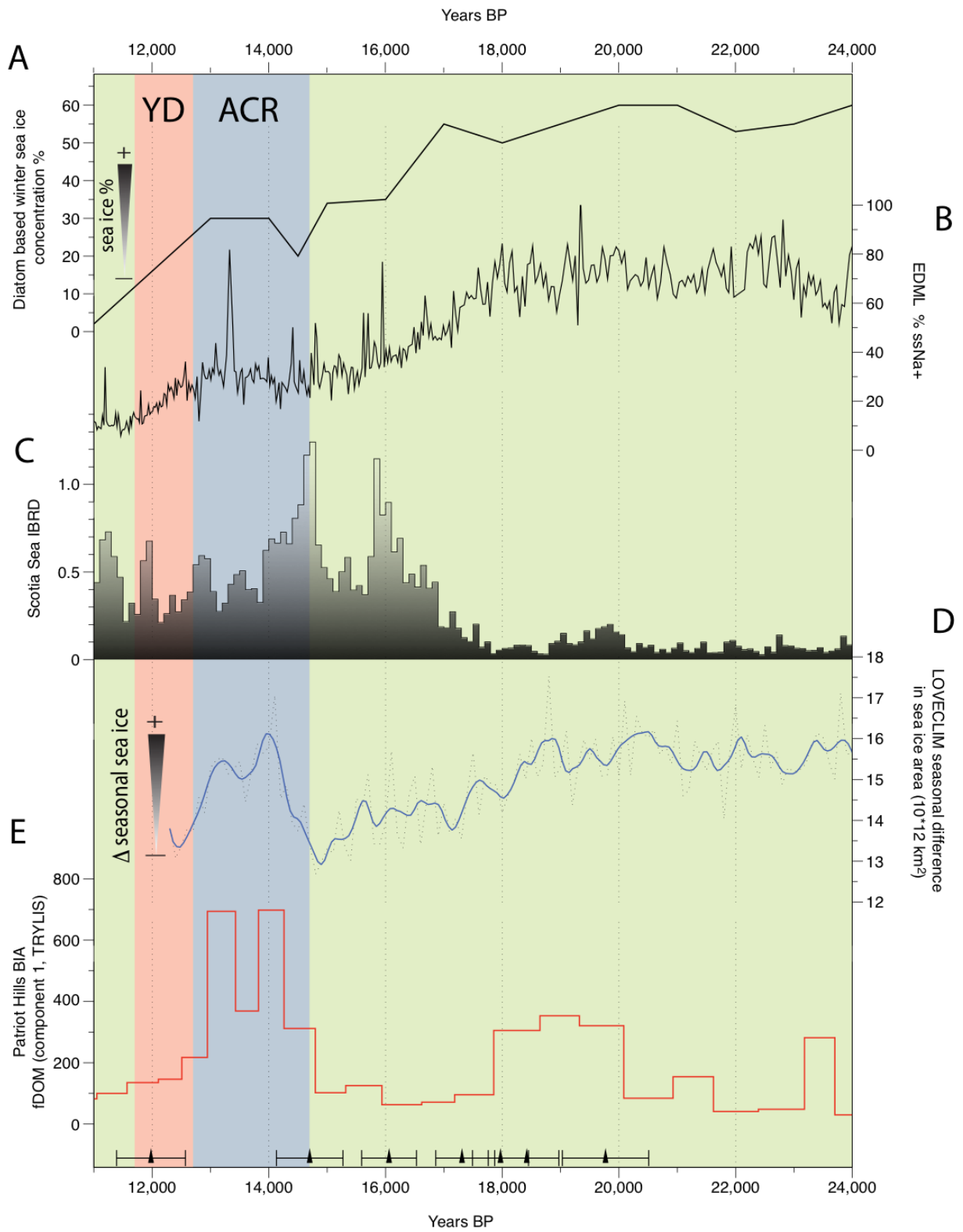
305 As recorded in contemporary mesoscale experiments picoplankton and picoeukaryotes form the  
306 basis of the pelagic communities response to iron fertilisation in the high-latitude HLNC Southern  
307 Ocean(Boyd et al., 2000), and are key to CO<sub>2</sub> draw down in the polar Southern Ocean(Boyd et al.,  
308 2019). With Imaging Flow Cytometry and independent biomarker (fOM and LC-OCD) analysis  
309 demonstrating that the TRYLIS and TYLIS components identified are a measure of picoplankton  
310 and picoeukaryotes populations the fOM signal can be interpreted as a robust measure of Southern  
311 Ocean productivity in the Weddell and Scotia Sea areas of the South Atlantic sector of the Southern  
312 Ocean. With both the TRYLIS and TYLIS components being identified in the WAIS Divide  
313 core(Rohde et al., 2008) and in the fOM signal in contemporary snow cores from the Patriot Hills  
314 site that record the past decade (see Supplementary Information (Figures S1 and S2)), it provides a  
315 measure of high-latitude surface marine productivity in this sector of the Southern Ocean that can  
316 be linked to export production in the Southern Ocean (Boyd et al., 2000), a hypothesis testable  
317 through the analysis of marine sediments from sites such as The Scotia Sea.

318

## 319 **Results**

320 By comparing the records of fOM across the LGT we observe a pronounced peak in these  
321 biomarkers across the well-constrained ACR part of the Patriot Hills BIA sequence (Figure 5).  
322 This change in fOM signal could reflect marked changes in precipitation source over the LGT;  
323 however, regime shift analysis (Rodionov, 2004) on the deuterium-excess profile measured across

324 the LGT profile reveals no significant variability across the ACR, or the LGT, at either 99% or  
325 95% confidence, indicating that the precipitation source remained constant (Figure 3C). The  
326 implication is that the fOM signal reflects large relative variations in the concentration of TRYLIS  
327 and TYLIS in the precipitation source region produced by the aerial transport of marine  
328 microorganisms, principally nanoplankton, picoplankton and picoeukaryotes as identified through  
329 ImageSteam®. In our analysis, we focus on the variation in the TRYLIS component, which makes  
330 up highest percentage of the variance in fOM signal (83.33%: see Supplementary Information).  
331 The fOM TRYLIS component, hence concentration of marine-derived nanoplankton,  
332 picoplankton and picoeukaryotes, is highly variable across the BIA ice core record but has a  
333 sustained high concentration through the ACR (Figure 5E).



335 **Figure 5.** Comparison of A. Diatom transfer function-based estimates of winter sea-ice  
336 concentration (Esper and Gersonde, 2014), B. Sea salt (ssNa<sup>+</sup>) from EPICA Dronning Maud Land  
337 (EDML) (Wolff et al., 2006a). C. Iceberg-rafted debris flux (IBRD; normalised 100-year average)  
338 relative to Holocene from core MD07-3134 (Weber et al., 2014). D. Difference in seasonal extent  
339 of Antarctic sea-ice area from LOVECLIM (Menviel et al., 2011) and E. fOM concentration  
340 (Component 1; TRYLIS, raw data is represented by a solid red line). Vertical boxes indicate the  
341 periods defined by the Antarctic Cold Reversal (ACR) (blue), the Younger Dryas (YD)  
342 chronozone (11.7-12.7 ka) and black triangles represent the age tie points (derived from  
343 geochemically identified volcanic horizons and trace gases, see Supplementary Information and  
344 Figure S1) in this section of the Patriot Hills BIA (see Figure 3).

345  
346 To further investigate the detail of the marine biomarker signals, large volume ice samples were  
347 sampled across the LGT portion of the exposed BIA at Patriot Hills to extract ancient bacterial  
348 DNA *in situ* by directly melting and filtering samples from specific time-horizons – a novel  
349 approach to minimize the introduction of contaminants (see Supplementary Information) and  
350 which enables us to obtain insights into the picoplankton, picoeukaryotes and nanoplankton  
351 represented at a taxa level. 16S rRNA indexing reveals a marked ecological switch characterized  
352 by the appearance of large numbers of halotolerant microorganisms commonly found in seawater  
353 was observed during the ACR, coincident with the increase in fOM TRYLIS signal (Figure 4C  
354 (see Supplementary Information (Tables S1 and S2)). Specifically, we found marine-associated  
355 taxa, *Helicobacteraceae*, *Rhodobacteraceae*, *Marinobacter* and *Pseudidiomarina*, statistically  
356 associated with the ACR period ( $p < 0.038$ ), and observe a slight increase in species diversity  
357 (predominantly marine taxa) compared to that observed during either the mid-Holocene or the

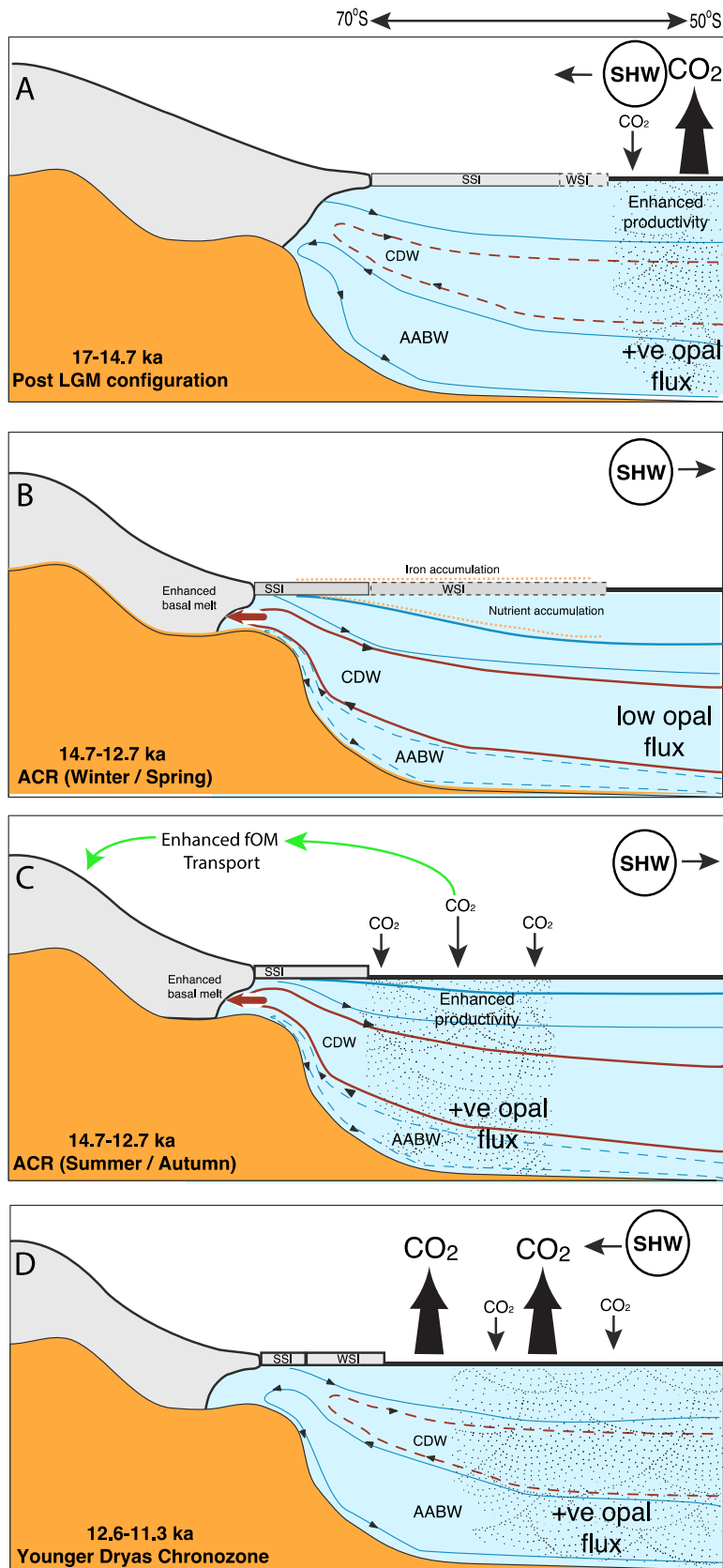
358 glacial samples from the Patriot Hills BIA sequence (Figure 5, Tables S1 and S2). Whilst the source  
359 of this signal could have been from brine pools associated with the build-up of sea ice, we suggest,  
360 based on the taxa identified, that the signal reflects an enhanced diversity and productivity from  
361 open marine, or marginal sea ice zone. With five independent approaches (LC-OCD, Imaging  
362 Flow Cytometry analysis, and the independent fOM and DNA) each pointing to enhanced marine  
363 biological productivity in the high latitude South Atlantic sector of the Southern Ocean our results  
364 infer that the ACR was a period of enhanced marine biological productivity. With the enhanced  
365 picoplankton and picoeukaryotes signals derived from the surface precipitation source waters of  
366 the HNLC Southern Ocean during the ACR, we suggest that there was a strengthening of the  
367 biological pump which mirrored the effects of iron-fertilisation(Boyd et al., 2000) in this South  
368 Atlantic Sector of the Southern Ocean, a finding that supports the enhanced export production  
369 recorded in marine sediments from the Scotia Sea (Figure 1E) (Weber et al., 2014).

370

## 371 **Discussion**

372 To reconcile the apparent conflict between the increase in marine productivity recorded in marine  
373 sediments from the Scotia Sea and the Patriot Hills ice core with the decrease reported further  
374 north in the South Atlantic (Anderson et al., 2009; Jaccard et al., 2016) during the ACR, we  
375 compare our record of marine biomarkers (fOM) captured in ice with potential drivers of Southern  
376 Ocean productivity. We compare available records of iceberg rafted debris (IBRD; a proxy for  
377 Antarctic iceberg discharge) (Weber et al., 2014)), sea salt sodium ( $ssNa^+$ ) from the EDML ice  
378 core (a proxy for sea-ice extent) (Wolff et al., 2006b), proxy sea-ice reconstructions (Abelmann et  
379 al., 2015; Esper and Gersonde, 2014) to investigate possible physical drivers of enhanced  
380 productivity, and we compare independent transient modelling experiments using LOVECLIM

381 that include fresh water hosing in the Ross and Weddell seas (Menviel et al., 2011) (Figure 5; and  
382 Supplementary Information). Comparison between these records and the BIA LGT record between  
383 ~24 and ~14.6 kyr BP indicate weak relationships between marine biological productivity (using  
384 opal flux as a measure of export production), sea-ice expansion, atmospheric CO<sub>2</sub> variability and  
385 the peak in marine derived biomarkers (fOM), agreeing with previous studies (Figure 5) (Collins  
386 et al., 2012). This contrasts with the period defined by the ACR, where we observe a strong  
387 relationship between marine fOM in the Patriot Hills BIA, increased production of biogenic opal  
388 in the Scotia Sea, and the extended atmospheric CO<sub>2</sub> plateau across the ACR (Figures 1 and 5).  
389 Given that this increase in marine productivity seen in the Scotia Sea during the ACR is not  
390 apparent in mid-latitude marine records (Figure 2)(Anderson et al., 2009; Jaccard et al., 2016), we  
391 focus on possible high-latitude drivers of CO<sub>2</sub> exchange: iron fertilization from enhanced IBRD  
392 flux (Duprat et al., 2016), a reduction in Antarctic Bottom Water (AABW) formation due to  
393 enhanced freshwater flux (Fogwill et al., 2015; Golledge et al., 2014; Menviel et al., 2010), and  
394 sea-ice feedbacks (Abelmann et al., 2015) (Figure 6).



396 **Figure 6.** Schematic cross section of the mid to high latitude Southern Ocean. A. Post-Last Glacial  
397 Maximum (LGM) configuration with southerly displacement of the Southern Hemisphere  
398 Westerlies (SHW), depicting enhanced overturning of mid-latitude Southern Ocean between ~17  
399 ka- 14.7 ka as suggested by opal flux (Anderson et al., 2009). B. Antarctic Cold Reversal with  
400 enhanced intrusion of Circumpolar Deepwater (CDW) onto Antarctic shelf areas. Austral winter /  
401 spring, depicts marked winter sea-ice expansion (WSI), northwards migration of the SHW, with  
402 stratification and deepening of the mixed layer allowing ‘nutrient refuelling’ from deeper nutrient-  
403 enriched ocean and reduction in AABW formation at high-latitudes (Abelmann et al., 2015). C.  
404 Antarctic Cold Reversal (austral summer/autumn), extensive WSI break up enhancing marine  
405 primary productivity, from light and iron fertilization in a warming ocean leading to enhanced CO<sub>2</sub>  
406 drawdown in high-latitude HNLC Southern Ocean. D. Younger Dryas chronozone mid-latitude  
407 overturning reinvigorated leading to degassing of old carbon, and enhanced opal flux across the  
408 Southern Ocean.

409

410 IBRD contains high concentrations of bioavailable iron, making iceberg melt a potential source  
411 for increased primary productivity and carbon sequestration through fertilization across the HNLC  
412 regions of the high-latitude Southern Ocean (Duprat et al., 2016). Intriguingly, despite significant  
413 evidence for potential enhanced iron fertilization of the Southern Ocean through increased delivery  
414 of IBRD at around 20-19 kyr BP and 17-16 kyr BP (Weber et al., 2014), there does not seem to be  
415 a strong biological response in the Patriot Hills fOM or Scotia Sea opal flux records (Figures 2 and  
416 5), suggesting enhanced IRBD influx did not lead to enhanced high-latitude marine export  
417 production.

418



419 Alternatively, an increase in meltwater flux and reduction in the rate of AABW formation during  
420 the ACR (Golledge et al., 2014; Menviel et al., 2011; Menviel et al., 2016; Weber et al., 2014)  
421 may have increased stratification and carbon sequestration across the high-latitude Southern  
422 Ocean. Published analysis has demonstrated that there was significant ice-sheet drawdown across  
423 the Weddell Sea Embayment at this time (Fogwill et al., 2017; Weber et al., 2014), suggesting that  
424 influx of meltwater could have triggered stratification, and substantial circulation changes across  
425 the broader Southern Ocean, magnified by associated shifts in the intensity and/or location of  
426 surface westerly air flow (Anderson et al., 2009; Fogwill et al., 2017; Hogg et al., 2016; Jaccard  
427 et al., 2016). This interpretation is supported by independent ice-sheet and Earth system modelling  
428 experiments (Menviel et al., 2011; Weber et al., 2014). However, the disparity in the opal flux  
429 records between marine cores from the mid-latitude South Atlantic (Anderson et al., 2009) and  
430 Scotia Sea, suggests that the enhanced export production was focussed on the high-latitude South  
431 Atlantic during the ACR (Figure 1).

432  
433 An alternative mechanism that could enhance marine productivity at the high-latitudes involves  
434 sea-ice feedbacks. Recent studies of full glacial conditions suggest that reduced surface–deep  
435 ocean exchange and enhanced nutrient consumption by phytoplankton in the Southern Ocean may  
436 have lowered atmospheric CO<sub>2</sub> (Abelmann et al., 2015; Collins et al., 2012). During the austral  
437 winter, sea-ice expansion allowed the mixed layer to deepen, ‘refuelling’ the surface ocean with  
438 nutrients from the deep ocean reservoir, and enhancing near-surface productivity and export  
439 production during the break up of sea ice in the subsequent summer. This process was likely  
440 amplified by the addition of iron from sea-ice melt and breakup in the post-glacial HNLC ocean,  
441 and possibly seasonal temperature changes and CaCO<sub>3</sub> dissolution (Delille et al., 2014).

442

443 The strong marine fOM signal preserved in the Patriot Hills BIA coincides with Southern  
444 Hemisphere surface ocean and atmosphere cooling during the ACR (Figure 5). Proxy records and  
445 transient Earth system modelling (Menviel et al., 2011) suggest the highest seasonal variability in  
446 sea-ice extent across the LGT took place during the ACR (with greatest extent during winter and  
447 spring) (Figure 5), implying these sea-ice feedbacks were amplified across this period (Figure 6).  
448 The conditions contrast markedly in the periods immediately prior to (Figure 6A) and following  
449 (Figure 6D) the ACR, when the seasonal sea ice zone was relatively less variable (Figure 5), the  
450 high-latitude Southern Ocean less stratified (Golledge et al., 2014; Menviel et al., 2011; Weber et  
451 al., 2014), and the location of the Intertropical Convergence Zone (ITCZ) and mid-latitude  
452 Southern Hemisphere Westerlies were relatively further south (Figure 2). Set against a backdrop  
453 of a warming ocean during the LGT this likely created ideal conditions for enhanced Southern  
454 Ocean productivity in the high-latitude Southern Ocean, especially in sectors of the South Atlantic  
455 such as the Weddell and Scotia seas.

456

457 Comparison between our continuous Scotia Sea opal flux record (Weber et al., 2014) and the  
458 Patriot Hills BIA fOM record suggests that we are capturing a high-latitude signal of enhanced  
459 surface marine primary productivity caused by marked seasonal sea-ice variability during the  
460 ACR, a period characterised by a sustained atmospheric CO<sub>2</sub> plateau (Jaccard et al., 2016; Marcott  
461 et al., 2014; Schmitt et al., 2012). During the ACR, most marine records across the mid-latitudes  
462 suggest the biological pump in the Southern Ocean weakened, in apparent contradiction of the  
463 plateau in atmospheric CO<sub>2</sub> at that time (Figure 2). Our results indicate that despite low dust input  
464 (Figure 2), and surface cooling across subantarctic waters during the ACR, marked variability in

465 sea-ice extent resulted in increased seasonal surface productivity in the HNLC waters of the high-  
466 latitude South Atlantic sector of the Southern Ocean in comparison to periods prior to and  
467 following this event (Figure 5). We suggest that increased seasonal marine primary productivity  
468 in fact enhanced the Southern Ocean organic carbon pump, increasing carbon drawdown (and  
469 leading to enhanced export production) (Figure 6). Whilst other mechanisms may have played a  
470 part in the 1,900 year-long ACR CO<sub>2</sub> plateau – including iron fertilization, cool Southern Ocean  
471 surface temperatures and possibly reductions in the rate of AABW formation – the potential that  
472 seasonal Southern Ocean sea-ice feedbacks in the South Atlantic sector of the high-latitude  
473 Southern Ocean may have contributed to a slowdown in the rate of CO<sub>2</sub> rise during the ACR is a  
474 significant observation that has implications for our understanding of the role of the Southern  
475 Ocean in global carbon dynamics. Crucially, our results imply that during periods of Southern  
476 Ocean sea-ice expansion, high variability in winter and summer sea-ice extent may result in  
477 enhanced carbon sequestration as seen recently , providing a negative feedback during periods of  
478 rising CO<sub>2</sub>, a finding that requires detailed assessment given contemporary Antarctic sea ice  
479 changes (Barnes, 2015).

480

481 **Acknowledgments:** CJF, CSMT, LM, NRG, LSW and AC are supported by their respective  
482 Australian Research Council (ARC) and Royal Society of NZ fellowships, and CJF and AC thanks  
483 Keele University for a Research Development Award that underpinned this research at Keele  
484 University ICELAB and Exeter University. Fieldwork was undertaken under ARC Linkage Project  
485 (LP120200724), supported by Linkage Partner Antarctic Logistics and Expeditions whose support  
486 we gratefully acknowledge. CSIRO's contribution was supported in part by the Australian Climate  
487 Change Science Program (ACCSP), an Australian Government Initiative. SMD acknowledges

488 financial support from Coleg Cymraeg Cenedlaethol and the European Research Council (ERC  
489 grant agreement no. 25923). MEW acknowledges support from the Deutsche  
490 Forschungsgemeinschaft (grant We2039/8-1). The data reported in this paper are archived on the  
491 NOAA Paleoclimatology website. There are no competing interests.

492

493 **Author contribution:** CJF, CSMT, AB and AC conceived this research. CJF, CSMT, AB, MEW,  
494 DE, MR DPT, TDvO, ADM, MAJC, SD, MB, NCM, JV, AR, LM, HM, CM, JY, MM, AC, MH,  
495 AP, JL, LSW and AC undertook analysis and sampling. CJF, CSMT, AB, MEW and AC wrote  
496 the manuscript with input from all the authors.

497

498 **Data availability:** The Patriot Hills  $\delta d$  and  $\delta^{18}O$  isotope data, and the age model is available at  
499 National Oceanic and Atmospheric Administration Paleoclimatology Database  
500 (<https://www.ncdc.noaa.gov/paleo/study/21691>), and the data from core MD07-3134 are available  
501 at <http://dx.doi.org/10.1594/PANGAEA.819646>. The biomarker and DNA data will be made  
502 available upon publication through the NOAA archive.

503

504 **Additional Information:**

505 The authors declare no competing interests. Supplementary information accompanies this paper at  
506 [www.xxxxxxx](http://www.xxxxxxx). Correspondence and requests for materials should be addressed to C.J.F.  
507 [c.j.fogwill@keele.ac.uk](mailto:c.j.fogwill@keele.ac.uk).

508

509

510

511

512

513

514

515 **References**

- 516 Abelmann, A., Gersonde, R., Knorr, G., Zhang, X., Chaplign, B., Maier, E., Esper, O.,  
517 Friedrichsen, H., Lohmann, G., Meyer, H., and Tiedemann, R., 2015, The seasonal sea-  
518 ice zone in the glacial Southern Ocean as a carbon sink: *Nature Communications*, v. 6, p.  
519 8136.
- 520 Abram, N. J., Mulvaney, R., Wolff, E. W., and Mudelsee, M., 2007, Ice core records as sea ice  
521 proxies: An evaluation from the Weddell Sea region of Antarctica: *Journal of*  
522 *Geophysical Research*, v. 112, no. D15101.
- 523 Anderson, R. F., Ali, S., Bradtmiller, L. I., Nielsen, S. H. H., Fleisher, M. Q., Anderson, B. E.,  
524 and Burckle, L. H., 2009, Wind-Driven Upwelling in the Southern Ocean and the  
525 Deglacial Rise in Atmospheric CO<sub>2</sub>: *Science*, v. 323, no. 5920, p. 1443-1448.
- 526 Barker, J. D., Dubnick, A., Lyons, W. B., and Chin, Y.-P., 2013, Changes in Dissolved Organic  
527 Matter (DOM) Fluorescence in Proglacial Antarctic Streams: *Arctic, Antarctic and*  
528 *Alpine Research*, v. 45, no. 3, p. 305-317.
- 529 Barnes, D. K. A., 2015, Antarctic sea ice losses drive gains in benthic carbon drawdown: *Current*  
530 *Biology*, v. 25, no. 18, p. R789-R790.
- 531 Bauska, T. K., Baggenstos, D., Brook, E. J., Mix, A. C., Marcott, S. A., Petrenko, V. V.,  
532 Schaefer, H., Severinghaus, J. P., and Lee, J. E., 2016, Carbon isotopes characterize rapid  
533 changes in atmospheric carbon dioxide during the last deglaciation: *Proceedings of the*  
534 *National Academy of Sciences*, v. 113, no. 13, p. 3465-3470.
- 535 Boyd, P. W., Claustre, H., Levy, M., Siegel, D. A., and Weber, T., 2019, Multi-faceted particle  
536 pumps drive carbon sequestration in the ocean: *Nature*, v. 568, no. 7752, p. 327-335.
- 537 Boyd, P. W., Watson, A. J., Law, C. S., Abraham, E. R., Trull, T., Murdoch, R., Bakker, D. C.  
538 E., Bowie, A. R., Buesseler, K. O., Chang, H., Charette, M., Croot, P., Downing, K.,  
539 Frew, R., Gall, M., Hadfield, M., Hall, J., Harvey, M., Jameson, G., LaRoche, J.,  
540 Liddicoat, M., Ling, R., Maldonado, M. T., McKay, R. M., Nodder, S., Pickmere, S.,  
541 Pridmore, R., Rintoul, S., Safi, K., Sutton, P., Strzepak, R., Tanneberger, K., Turner, S.,  
542 Waite, A., and Zeldis, J., 2000, A mesoscale phytoplankton bloom in the polar Southern  
543 Ocean stimulated by iron fertilization: *Nature*, v. 407, p. 695.
- 544 Butterworth, B. J., and Miller, S. D., 2016, Air-sea exchange of carbon dioxide in the Southern  
545 Ocean and Antarctic marginal ice zone. : *Geophysical Research Letters*, v. 43, p. 7223-  
546 7230.
- 547 Collins, L. G., Pike, J., Allen, C. S., and Hodgson, D. A., 2012, High-resolution reconstruction of  
548 southwest Atlantic sea-ice and its role in the carbon cycle during marine isotope stages 3  
549 and 2: *Paleoceanography*, v. 27, no. 3, p. PA3217.
- 550 D'Andrilli, J., Foreman, C. M., Sigl, M., Priscu, J. C., and McConnell, J. R., 2016, A 21,000 year  
551 record of organic matter quality in the WAIS Divide ice core: *Clim. Past Discuss.*, v.  
552 2016, p. 1-15.
- 553 Delille, B., Vancoppenolle, M., Geilfus, N.-X., Tilbrook, B., Lannuzel, D., Schoemann, V.,  
554 Becquevort, S., Carnat, G., Delille, D., Lancelot, C., Chou, L., Dieckmann, G. S., and  
555 Tison, J.-L., 2014, Southern Ocean CO<sub>2</sub> sink: The contribution of the sea ice: *Journal of*  
556 *Geophysical Research: Oceans*, v. 119, no. 9, p. 6340-6355.
- 557 Duprat, L. P. A. M., Bigg, G. R., and Wilton, D. J., 2016, Enhanced Southern Ocean marine  
558 productivity due to fertilization by giant icebergs: *Nature Geosci*, v. 9, p. 219-221.

- 559 Esper, O., and Gersonde, R., 2014, New tools for the reconstruction of Pleistocene Antarctic sea  
560 ice: *Palaeogeography, Palaeoclimatology, Palaeoecology*, v. 399, p. 260-283.
- 561 Fogwill, C., Turney, C., Golledge, N., Etheridge, D., Rubino, M., Thornton, D., Baker, A.,  
562 Woodward, J., Winter, K., and Van Ommen, T., 2017, Antarctic ice sheet discharge  
563 driven by atmosphere-ocean feedbacks at the Last Glacial Termination: *Scientific reports*,  
564 v. 7, p. 39979.
- 565 Fogwill, C. J., and Kubik, P. W., 2005, A glacial stage spanning the Antarctic Cold Reversal in  
566 Torres del Paine (51 degrees S), Chile, based on preliminary cosmogenic exposure ages:  
567 *Geografiska Annaler Series a-Physical Geography*, v. 87A, no. 2, p. 403-408.
- 568 Fogwill, C. J., Phipps, S. J., Turney, C. S. M., and Golledge, N. R., 2015, Sensitivity of the  
569 Southern Ocean to enhanced regional Antarctic ice sheet meltwater input: *Earth's Future*,  
570 v. 3, no. 10, p. 317-329.
- 571 Golledge, N. R., Menviel, L., Carter, L., Fogwill, C. J., England, M. H., Cortese, G., and Levy,  
572 R. H., 2014, Antarctic contribution to meltwater pulse 1A from reduced Southern Ocean  
573 overturning: *Nat Commun*, v. 5.
- 574 Gottschalk, J., Skinner, L. C., Lippold, J., Vogel, H., Frank, N., Jaccard, S. L., and Waelbroeck,  
575 C., 2016, Biological and physical controls in the Southern Ocean on past millennial-scale  
576 atmospheric CO<sub>2</sub> changes.: *Nat Commun*, v. 7, no. 11539.
- 577 Hewitt, A. J., Booth, B. B. B., Jones, C. D., Robertson, E. S., Wiltshire, A. J., Sansom, P. G.,  
578 Stephenson, D. B., and Yip, S., 2016, Sources of uncertainty in future projections of the  
579 carbon cycle.: *Journal of Climate*, v. 29, p. 7203-7213.
- 580 Hogg, A., Southon, J., Turney, C., Palmer, J., Bronk Ramsey, C., Fenwick, P., Boswijk, G.,  
581 Friedrich, M., Helle, G., Hughen, K., Jones, R., Kromer, B., Noronha, A., Reynard, L.,  
582 Staff, R., and Wacker, L., 2016, Punctuated shutdown of Atlantic Meridional Overturning  
583 Circulation during the Greenland Stadial 1: *Scientific Reports*, v. 6, no. 25902.
- 584 Hood, E., Fellman, J., Spencer, R. G. M., Hernes, P. J., Edwards, R., D'Amore, D., and Scott,  
585 D., 2009, Glaciers as a source of ancient and labile organic matter to the marine  
586 environment: *Nature*, v. 462, no. 7276, p. 1044-1047.
- 587 Huber, S. A., Balz, A., Abert, M., and Pronk, W., 2011, Characterisation of aquatic humic and  
588 non-humic matter with size-exclusion chromatography – organic carbon detection –  
589 organic nitrogen detection (LC-OCD-OND): *Water Research*, v. 45, no. 2, p. 879-885.
- 590 Jaccard, S. L., Galbraith, E. D., Martínez-García, A., and Anderson, R. F., 2016, Covariation of  
591 deep Southern Ocean oxygenation and atmospheric CO<sub>2</sub> through the last ice age: *Nature*,  
592 v. 530, p. 207-210.
- 593 Jaccard, S. L., Hayes, C. T., Martínez-García, A., Hodell, D. A., Anderson, R. F., Sigman, D. M.,  
594 and Haug, G. H., 2013, Two Modes of Change in Southern Ocean Productivity Over the  
595 Past Million Years: *Science*, v. 339, no. 6126, p. 1419-1423.
- 596 Jørgensen, L., Stedmon, C. A., Kragh, T., Markager, S., Middelboe, M., and Søndergaard, M.,  
597 2011, Global trends in the fluorescence characteristics and distribution of marine  
598 dissolved organic matter: *Marine Chemistry*, v. 126, no. 1, p. 139-148.
- 599 King, A., Wolff, E., Thomas, E., Kalberer, M., Giorio, C., and MargitSchwikowski, 2019, Novel  
600 organic compounds in ice cores for use in paleoclimatereconstruction: *Geophysical*  
601 *Research Abstracts*, , v. EGU General Assembly 2019, no. CL1.11/CR5.6
- 602 Le Quéré, C., Rödenbeck, C., Buitenhuis, E. T., Conway, T. J., Langenfelds, R., Gomez, A.,  
603 Labuschagne, C., Ramonet, M., Nakazawa, T., Metz, N., Gillett, N., and Heimann, M.,

- 604 2007, Saturation of the Southern Ocean CO<sub>2</sub> sink due to recent climate change. : Science,  
605 v. 316, p. 1735-1738.
- 606 Marcott, S. A., Bauska, T. K., Buizert, C., Steig, E. J., Rosen, J. L., Cuffey, K. M., Fudge, T. J.,  
607 Severinghaus, J. P., Ahn, J., Kalk, M. L., McConnell, J. R., Sowers, T., Taylor, K. C.,  
608 White, J. W. C., and Brook, E. J., 2014, Centennial-scale changes in the global carbon  
609 cycle during the last deglaciation: Nature, v. 514, no. 7524, p. 616-619.
- 610 Marshall, J., and Speer, K., 2012, Closure of the meridional overturning circulation through  
611 Southern Ocean upwelling. : Nature Geoscience, v. 5, p. 171-180.
- 612 Martínez-García, A., Sigman, D. M., Ren, H., Anderson, R. F., Straub, M., Hodell, D. A.,  
613 Jaccard, S. L., Eglinton, T. I., and Haug, G. H., 2014, Iron Fertilization of the  
614 Subantarctic Ocean During the Last Ice Age: Science, v. 343, no. 6177, p. 1347-1350.
- 615 McGlone, M. S., Turney, C. S. M., Wilmshurst, J. M., Renwick, J., and Pahnke, K., 2010,  
616 Divergent trends in land and ocean temperature in the Southern Ocean over the past  
617 18,000 years: Nature Geosci, v. 3, no. 9, p. 622-626.
- 618 Menviel, L., A. Timmermann, O. Elison Timm, and Mouchet, A., 2011, Deconstructing the Last  
619 Glacial Termination: the role of millennial and orbital-scale forcings: Quaternary Science  
620 Reviews, v. 30, p. 1155-1172.
- 621 Menviel, L., J. Yu, F. Joos, A. Mouchet, K. J. Meissner, and England, M. H., 2016, Poorly  
622 ventilated deep ocean at the Last Glacial Maximum inferred from carbon isotopes: A  
623 data-model comparison study.: Paleoceanography, v. 31.
- 624 Menviel, L., Timmermann, A., Timm, O. E., and Mouchet, A., 2010, Climate and  
625 biogeochemical response to a rapid melting of the West Antarctic Ice Sheet during  
626 interglacials and implications for future climate: Paleoceanography, v. 25, no. 4, p.  
627 PA4231.
- 628 Meyer-Jacob, C., Vogel, H., Boxberg, F., Rosén, P., Weber, M., and Bindler, R., 2014,  
629 Independent measurement of biogenic silica in sediments by FTIR spectroscopy and PLS  
630 regression: Journal of Paleolimnology, v. 52, no. 3, p. 245-255.
- 631 Monnin, E., Indermöhle, A., Dällenbach, A., Flückiger, J., Stauffer, B., Stocker, T. F.,  
632 Raynaud, D., and Barnola, J.-M., 2001, Atmospheric CO<sub>2</sub> Concentrations over the Last  
633 Glacial Termination: Science, v. 291, no. 5501, p. 112-114.
- 634 Muller, C. L., Baker, A., Hutchinson, R., Fairchild, I. J., and Kidd, C., 2008, Analysis of  
635 rainwater dissolved organic carbon compounds using fluorescence spectrometry. :  
636 Atmospheric Environment, v. 34, p. 8036-8045.
- 637 Orsi, A. H., III, T. W., and W. D. Nowlin, J., 1995, On the meridional extent and fronts of the  
638 Antarctic Circumpolar Current,: Deep-Sea Research, v. 1, no. 42, p. 641-673.
- 639 Parlanti, E., Wörz, K., Geoffroy, L., and Lamotte, M., 2000, Dissolved organic matter  
640 fluorescence spectroscopy as a tool to estimate biological activity in a coastal zone  
641 submitted to anthropogenic inputs: Organic Geochemistry, v. 31, no. 12, p. 1765-1781.
- 642 Pedro, J. B., Bostock, H. C., Bitz, C. M., He, F., Vandergoes, M. J., Steig, E. J., Chase, B. M.,  
643 Krause, C. E., Rasmussen, S. O., Markle, B. R., and Cortese, G., 2015, The spatial extent  
644 and dynamics of the Antarctic Cold Reversal: Nature Geosci, v. 9, p. 51-55  
645 .
- 646 Reijmer, C. H., Greuell, W., and Oerlemans, J., 1999, The annual cycle of meteorological  
647 variables and the surface energy balance on Berkner Island, Antarctica,: Ann. Glaciol., v.  
648 29, p. 49-54.



- 649 Rodionov, S. N., 2004, A sequential algorithm for testing climate regime shifts: *Geophys. Res.*  
650 *Let.*, v. 31, no. L09204.
- 651 Rohde, R. A., Price, P. B., Bay, R. C., and Bramall, N. E., 2008, *In situ* microbial  
652 metabolism as a cause of gas anomalies in ice: *Proceedings of the National Academy of*  
653 *Sciences*, v. 105, no. 25, p. 8667-8672.
- 654 Schmitt, J., Schneider, R., Elsig, J., Leuenberger, D., Lourantou, A., Chappellaz, J., Köhler, P.,  
655 Joos, F., Stocker, T. F., Leuenberger, M., and Fischer, H., 2012, Carbon Isotope  
656 Constraints on the Deglacial CO<sub>2</sub> Rise from Ice Cores: *Science*, v. 336, no. 6082, p. 711-  
657 714.
- 658 Smith, H. J., Foster, R. A., McKnight, D. M., Lisle, J. T., Littmann, S., Kuypers, M. M. M., and  
659 Foreman, C. M., 2017, Microbial formation of labile organic carbon in Antarctic glacial  
660 environments: *Nature Geosci*, v. 10, no. 5, p. 356-359.
- 661 Sprenk, D., Weber, M. E., Kuhn, G., Rosén, P., Frank, M., Molina-Kescher, M., Liebetrau, V.,  
662 and Röhling, H.-G., 2013, Southern Ocean bioproductivity during the last glacial cycle –  
663 new decadal-scale insight from the Scotia Sea: *Geological Society, London, Special*  
664 *Publications*, v. 381, no. 1, p. 245-261.
- 665 Stedmon, C. A., Markager, S., and Bro, R., 2003, Tracing dissolved organic matter in aquatic  
666 environments using a new approach to fluorescence spectroscopy.: *Marine Chemistry*, v.  
667 82, p. 239–254.
- 668 Toggweiler, J. R., Russell, J. L., and Carson, S. R., 2006, Midlatitude westerlies, atmospheric  
669 CO<sub>2</sub>, and climate change during the ice ages: *Paleoceanography*, v. 21, no. 2.
- 670 Turney, C. S. M., Fogwill, C. J., Van Ommen, T. D., Moy, A. D., Etheridge, D., Rubino, M.,  
671 Curran, M. A. J., and A., R., 2013, Late Pleistocene and early Holocene change in the  
672 Weddell Sea: a new climate record from the Patriot Hills, Ellsworth Mountains, West  
673 Antarctica: *Journal of Quaternary Science*, v. 28, no. 7, p. 697-704.
- 674 Turney, C. S. M., Palmer, J., Hogg, A., Fogwill, C. J., Jones, R. T., Bronk Ramsey, C., Fenwick,  
675 P., Grierson, P., Wilmshurst, J., O'Donnell, A., Thomas, Z. A., and Lipson, M., 2016,  
676 Multidecadal variations in Southern Hemisphere atmospheric <sup>14</sup>C: Evidence against a  
677 Southern Ocean sink at the end of the Little Ice Age CO<sub>2</sub> anomaly: *Global*  
678 *Biogeochemical Cycles*, v. 30, no. 2, p. 211-218.
- 679 Weber, M. E., Clark, P. U., Kuhn, G., Timmermann, A., Sprenk, D., Gladstone, R., Zhang, X.,  
680 Lohmann, G., Menviel, L., Chikamoto, M. O., Friedrich, T., and Ohlwein, C., 2014,  
681 Millennial-scale variability in Antarctic ice-sheet discharge during the last deglaciation:  
682 *Nature*, v. 510, no. 7503, p. 134-138.
- 683 Wessel, P. a. S., W.H., , 1998, New, improved version of Generic Mapping Tools released.: *Eos*,  
684 *Transactions American Geophysical Union*, v. 79, no. 47, p. 579-579.
- 685 Willey, J. D., Kieber, R.J., Eyman, M.S., Avery Jr., G.B., 2, 2000, Rainwater dissolved organic  
686 carbon: concentrations and global flux. : *Global Biogeochemical Cycles*, v. 14, p. 139–  
687 148.
- 688 Winter, K., Woodward, J., Dunning, S. A., Turney, C. S., Fogwill, C. J., Hein, A. S., Golledge,  
689 N. R., Bingham, R. G., Marrero, S. M., and Sugden, D. E., 2016a, Assessing the  
690 continuity of the blue ice climate record at Patriot Hills, Horseshoe Valley, West  
691 Antarctica: *Geophysical Research Letters*, v. 43, no. 5, p. 2019-2026.
- 692 Winter, K., Woodward, J., Dunning, S. A., Turney, C. S. M., Fogwill, C. J., Hein, A. S., Golledge,  
693 N. R., Bingham, R. G., Marrero, S. M., Sugden, D. E., and Ross, N., 2016b, Assessing the

694 continuity of the blue ice climate record at Patriot Hills, Horseshoe Valley, West  
695 Antarctica: *Geophys. Res. Lett.*, v. 10.1002/2015GL066476.

696 Wolff, E., Fischer, H., Fundel, F., Ruth, U., Twarloh, B., Littot, G., Mulvaney, R., Rothlisberger,  
697 R. d. A., M., Boutron, C., Hansson, M., Jonsell, U., Hutterli, M., Lambert, F., Kaufmann,  
698 P., Stauffer, B., Stocker, T., Steffensen, J., Bigler, M., Siggaard-Andersen, M., Udisti, R.,  
699 Becagli, S., Castellano, E., Severi, M., Wagenbach, D., Barbante, C., Gabrielli, P., and  
700 Gaspari, V., 2006a, Southern Ocean sea-ice extent, productivity and iron flux over the  
701 past eight glacial cycles. : *Nature*, v. 440, p. 491-496.

702 Wolff, E. W., Fischer, H., Fundel, F., Ruth, U., Twarloh, B., Littot, G. C., Mulvaney, R.,  
703 Röthlisberger, R., de Angelis, M., Boutron, C. F., Hansson, M., Jonsell, U., Hutterli, M.  
704 A., Lambert, F., Kaufmann, P., Stauffer, B., Stocker, T. F., Steffensen, J. P., Bigler, M.,  
705 Siggaard-Andersen, M. L., Udisti, R., Becagli, S., Castellano, E., Severi, M., Wagenbach,  
706 D., Barbante, C., Gabrielli, P., and Gaspari, V., 2006b, Southern Ocean sea-ice extent,  
707 productivity and iron flux over the past eight glacial cycles: *Nature*, v. 440, no. 7083, p.  
708 491-496.  
709

710

711

712

713

714

715

716

717

718

719

720